

The Metallicity Distribution in the Halo Stars of NGC 5128: Implications for Galaxy Formation

Gretchen L. H. Harris

Department of Physics, University of Waterloo
Waterloo ON L8S 3G1, Canada; glharris@astro.uwaterloo.ca

William E. Harris

Department of Physics and Astronomy, McMaster University
Hamilton ON L8S 4M1, Canada; harris@physics.mcmaster.ca

and

Gregory B. Poole

Department of Physics, University of Waterloo
Waterloo, ON N2L 3G1, Canada; gbpoole@astro.uwaterloo.ca

ABSTRACT

We have used the *Hubble Space Telescope* to obtain WFPC2 (V, I) photometry for stars in the halo of NGC 5128, the nearest giant elliptical galaxy. The resulting color-magnitude diagram (CMD) of this field, which lies ~ 21 kpc from the center of the galaxy, contains more than 10,000 stars and reaches almost 3 magnitudes down the red-giant branch (RGB). From the sharply defined RGB tip at $I = 24.1 \pm 0.1$ and $M_I(\text{tip}) = -4.1$, we obtain a distance to NGC 5128 of 3.9 Mpc. Comparison with the fiducial RGBs of Milky Way globular clusters and model isochrones demonstrates that this outer-halo population of NGC 5128 is completely dominated by old stars, with an extremely broad metallicity range extending from the most metal-poor Galactic globulars at $[\text{Fe}/\text{H}] \lesssim -2$ up to above-solar abundance. The relative contribution from any younger, bright asymptotic-branch component is negligible. The shape of the metallicity distribution function (MDF), derived from the CMD by interpolation within the isochrones, can be remarkably well matched by a simple two-component model of closed-box chemical enrichment, where the first component starts with an initial abundance $Z_0 = 0$ and the second component with $Z_0 \simeq 0.18Z_\odot$. Two-thirds of the stars belong to the metal-richer component

and one-third to the metal-poorer one; the mean metallicity of the entire sample is $\langle [\text{Fe}/\text{H}] \rangle = -0.41$, consistent with the colors of the integrated halo light. The metal-rich component also coincides strikingly in mean and dispersion with the metal-rich peak of the halo *globular clusters* in NGC 5128, suggesting that both of these halo subsystems formed contemporaneously. A discussion of various models of E galaxy formation leads us to suggest that a basic *in situ* formation picture with two distinct epochs of star formation best fits the observations; other models involving major contributions from accretions or mergers are less satisfactory. The timing of the events we suggest is that the first, more metal-poor star-forming epoch took place while the protogalaxy was still in a clumpy, fragmented state, leaving most of the gas unused. The second and larger star formation epoch took place after the majority of the now pre-enriched gas had recollected into the fully formed potential well of the new giant elliptical.

Subject headings: galaxies: elliptical and lenticular — galaxies: evolution — galaxies: abundances — galaxies: star clusters — galaxies: individual (NGC 5128)

1. Introduction

A color-magnitude diagram (CMD) for the stars in a galaxy is the definitive tool to establish the nature of its stellar population, and even a CMD limited to the brightest stars can provide considerable information on the nature of its star formation history. Such work is, however, difficult to carry out for the halos of galaxies because the old-halo stars are fainter than any Population I component, and can be directly resolved only for nearby galaxies. Thus for the most part, our knowledge of galaxy halos has been based on surface photometry of their integrated light. Particularly important exceptions are, of course, the Local Group members, notably M31 (e.g. Mould & Kristian 1986, Pritchett & van den Bergh 1988, Christian & Heasley 1991, Durrell et al. 1994, Reitzel et al. 1998) and the dwarf ellipticals (Grillmair et al. 1996, Han et al. 1997, Martinez-Delgado & Aparicio 1998). Recently, direct CMDs have been obtained from HST imaging of the halos of a small number of galaxies beyond the Local Group (Soria et al. 1996, Elson 1997, Caldwell et al. 1998).

What is missing entirely from the Local Group is the important giant elliptical class. Among all gE's, the closest one by far is NGC 5128, the dominant galaxy in the Centaurus group at $d \simeq 3.9$ Mpc (The next nearest gE target is NGC 3379 in the Leo group, more

than 2 magnitudes further away; while the rich collections of ellipticals in Virgo and Fornax are more than 3 magnitudes more distant). Although its central dust lane and gas, thought to be due to the recent accretion of a smaller satellite, have traditionally marked NGC 5128 as ‘peculiar’, its much larger main body and extensive outer halo resemble those of more nearly normal gE’s in structure, size, and color (Hui *et al.* 1995, Soria *et al.* 1996, Graham 1979, Ebneter & Balick 1983, van den Bergh 1976, Storchi-Bergmann *et al.* 1997). Since mergers and accretions of the type now going on in NGC 5128 are increasingly recognized as rather normal episodes in the histories of large galaxies, it is not unreasonable to expect that we can learn a great deal about the stellar populations in E galaxies by studying it intensively.

Though NGC 5128 is well beyond the Local Group, its halo red giant stars are clearly within reach of the Hubble Space Telescope cameras. To date, the only CMD study for the old-halo population of NGC 5128 is the work of Soria *et al.* (1996). But their CMD for a halo field about 10 kpc south of the center of NGC 5128 reaches only about 1.5 mag down the red-giant branch (RGB), and (as will be seen below) gives an incomplete picture of the full stellar distribution.

2. Observations

During HST Cycle 5 we obtained deep images of an outer-halo field in NGC 5128, located at a projected distance $R_{gc} = 18'.32$ south of the galaxy center (shown in Figure 1), equivalent to a linear distance of $20.8(d/3.9)$ kpc. For this program (GO-5905), ten orbits were assigned from the Cycle 5 competition in mid-1994, and the observations were executed three years later, in two visits on 1997 August 16 and 24. We used the WFPC2 camera in the two filters F606W (V) and F814W (I). Total exposures in each filter were 12800 sec (2×1200 sec + 8×1300 sec). The PC1 chip was centered on the halo globular cluster C44 (Harris *et al.* 1992, Hesser *et al.* 1986), as shown in Figure 2.

From the PC1 photometry we derived a CMD for the globular cluster, the first one for a globular cluster in any galaxy outside the Local Group; these results are described in Harris *et al.* (1998a). In the present paper, we discuss the main set of data from the three WF chips and the CMD for the halo stars.

Starting from the preprocessed images supplied by StScI, we reregistered all the individual exposures in each filter to a common coordinate system and combined them with the normal *stsdas.crrej* package. The exposures were sub-pixel shifted to facilitate the removal of cosmic rays, bad pixels, and other artifacts on the frames. Photometry on the

summed V and I frames was then carried out with the DAOPHOT II code (Stetson 1992). We defined the point spread function (PSF) using several moderately bright, isolated stars in each WF field, and carried out two iterations of the normal sequence of object finding and PSF fitting through ALLSTAR. Transformation of the instrumental magnitudes to V, I followed the prescriptions of Holtzman et al. (1995). No correction was made for the charge-transfer ramp effect across the frames (Holtzman *et al.* 1995, Whitmore & Heyer 1997) because of the length of our exposures. The final CMD in $(I, V - I)$, for 10,352 stars over the three WF fields combined, is shown in Figure 3a. Objects with goodness of fit $\chi > 2$ are excluded.

Artificial-star tests were then carried out to investigate the completeness of detection and the internal measurement uncertainty as functions of magnitude and color. The ADDSTAR code was used to add ~ 200 identical stars at a time to the WF2 frame for each color at 0.5-mag intervals across the CMD, and over a 7-magnitude range in I . The WF2 frame was chosen for the ADDSTAR tests because it had the smallest number of very bright stars and background galaxies. The “error bars” (internal measurement precisions σ_I, σ_{V-I}) resulting from these tests are shown in Figure 3b, along with the 90% and 50% detection completeness lines suitably transformed from the instrumental (v, i) magnitudes to the $(I, V - I)$ plane. Above the $f=0.9$ line, the data have photometric uncertainties $\sigma_I \lesssim <0.05$ mag and $\sigma_{V-I} \lesssim 0.1$ mag in $V - I$. Between the $f=0.9$ and 0.5 lines the data still have modest uncertainties $\lesssim 0.2$ mag in I and $\lesssim 0.3$ mag in $V - I$. The internal photometric errors increase very rapidly for completeness levels less than $f = 0.5$; in the following discussion, we will use none of the data fainter than this line, and almost none fainter than the $f = 0.9$ line.

A complete electronic file of the final photometry may be obtained on request from the first author.

3. The Color-Magnitude Diagram

The CMD in Figure 3a has several features that are immediately apparent. (1) The number of stars rises abruptly at $I \simeq 24.1$, which (like Soria et al. 1996) we interpret as the tip of the first-ascent red giant branch (TRGB). The value of I_{TRGB} has been shown to be a reliable distance indicator for old metal-poor stars (cf. Lee et al. 1993, Madore & Freedman 1995), and will be used in §4 below for a new calibration of the distance to NGC 5128. The following discussion will assume a distance of 3.9 Mpc, a foreground reddening of $E(V - I) = 0.14$, and thus an apparent distance modulus of $(m - M)_V = 28.2$. (2) The fact that the CMD contains almost no objects brighter than $I \sim 24$ indicates that the halo

at this location is dominated by an old stellar population, with little contamination from crowded stars or highly evolved bright AGB stars (e.g., Renzini 1998). (3) Over the $\lesssim 3$ magnitude range in I of our reliable data, the range in $V - I$ color is extremely broad – larger than has been seen in any other galaxy for which comparable data are available.

A primary goal of our study is to obtain the star-by-star *metallicity distribution function* (MDF) from the CMD. Giant ellipticals are known to have much higher mean metallicities than dwarfs or the halo of the Milky Way (e.g., Brodie & Huchra 1991, Kormendy & Djorgovski 1989, Thomsen & Baum 1989), extending up to solar $[\text{Fe}/\text{H}]$ and perhaps even higher. But what is the actual shape of the MDF which produces this high mean? As a first indication of the range of metallicities across the RGB, in Figure 4 we have superimposed the mean lines for standard Milky Way globular clusters of different metallicities (Da Costa & Armandroff 1990 and Guarnieri et al. 1998), shifted by our adopted reddening and distance modulus given above. These lines are for M15 ($[\text{Fe}/\text{H}] = -2.2$), NGC 1851 ($[\text{Fe}/\text{H}] = -1.3$), 47 Tuc ($[\text{Fe}/\text{H}] = -0.7$), and NGC 6553 ($[\text{Fe}/\text{H}] = -0.25$). Although the photometry for NGC 6553 (Guarnieri et al. 1998) is less precise and the locus less well defined than for the other clusters because of its crowding and high reddening ($E(B - V) = 0.7$), it is the most metal-rich globular cluster which we can call on with some level of confidence.

From the comparison in Figure 4, it is clear that the RGB stars extend fully from $[\text{Fe}/\text{H}] \sim -2.0$ to at least solar abundance and perhaps higher. A similar but not so obvious pattern appears in the CMD of Soria et al (1996; see their Figure 3). Blueward of the NGC 6397 ($[\text{Fe}/\text{H}] = -2.0$) locus, the number of bright giants diminishes markedly in their CMD but does not drop to zero. In our CMD, many stars fainter than $I \sim 26$ fall to the blue side of the M15 line; we interpret these as due to a combination of photometric scatter (Figure 3b) and the presence of AGB stars, whose tracks lie ~ 0.1 mag blueward of the RGB in this magnitude range.

We also compare our data with stellar models in Figure 5, using isochrones from Bertelli et al. (1994). More or less arbitrarily, we adopt their models for an age of 12.5 Gyr, and show the lines for their full range of metallicities, $[\text{Fe}/\text{H}] = -1.6$ to $+0.47$. Comparing these isochrones with the fiducial globular cluster lines in Figure 4, we find that the isochrones at $[\text{Fe}/\text{H}] \simeq -1.2$, -0.6 , and -0.3 match remarkably well with the fiducial cluster lines of similar metallicity. The $[\text{Fe}/\text{H}] = -1.6$ isochrone, in turn, matches well with M15 even though it is nominally 0.6 dex more metal-rich; we will not speculate here on the reasons for this. For the two most metal-rich isochrones at $[\text{Fe}/\text{H}] = +0.07$ and $+0.47$ we unfortunately have no direct observational comparison with real globular clusters. Observational scatter aside, the main conclusion to be drawn from Figures 4 and 5 is that this NGC 5128 halo field is dominated by an old stellar population with an extremely broad range in heavy

element abundance, possibly exceeding 2.0 dex.

It is also possible that star-to-star age differences may exist, and be responsible for some of the color spread. To explore the effect of age, in Figure 6 we compare the CMD with isochrones of various ages for a single metallicity, $[\text{Fe}/\text{H}] = -0.32$ (similar to the mean metallicity for the entire sample; see §6 below). This comparison demonstrates the conventional result that the color of the old RGB is affected much more strongly by metallicity than age; the observed color range in our data is far too great to be explained by a large range in age combined with a small or even moderate range in $[\text{Fe}/\text{H}]$. We conclude that the broad color range we observe must be due primarily to its range in chemical composition. This will be exploited further in §6 to derive the MDF.

4. The Brightest Stars and the Distance Calibration

The absolute magnitude of the RGB tip is well established as an excellent standard candle for stars with $[\text{Fe}/\text{H}] \lesssim -0.7$. Calibrations of the absolute I magnitude of the TRGB adjusted for recent Hipparcos parallax data give $M_I(\text{tip}) = -4.1 \pm 0.1$ (Mould & Kristian 1986, Lee et al. 1993, Madore & Freedman 1995, Sakai et al. 1996, Gratton et al. 1997, Harris et al. 1998b), which we adopt here. In Figure 7, we show the luminosity function of our entire dataset, as well as the LF for only those stars bluer than the $[\text{Fe}/\text{H}] = -0.6$ fiducial isochrone line in Figure 5. A rapid rise at $I_{\text{TRGB}} = 24.1 \pm 0.1$ is evident in both histograms. Although the calibration $M_I(\text{tip}) = -4.1$ applies strictly to the more metal-poor stars, it can be used for the whole LF over all metallicities just as well (knowing *a priori*, of course, that a significant population of low-metallicity stars is present). With $I_{\text{TRGB}} = 24.1 \pm 0.1$, $M_I = -4.1 \pm 0.1$, $E(B - V) = 0.11$ (Burstein & Heiles 1984) and thus $E(V - I) = 0.14$, $A_I = 0.22$, we therefore calculate a distance modulus of $(m - M)_0 = 27.98 \pm 0.15$, or $d = (3.9 \pm 0.3)$ Mpc. This estimate agrees well with the planetary nebula luminosity function value of $(m - M)_0 = 27.97 \pm 0.14$ (Hui *et al.* 1993); we have adjusted their published value upward by 0.2 mag to correct it to the contemporary Local Group distance scale, $(m - M)_0(\text{M31}) = 24.5$ (van den Bergh 1995, Fernley et al. 1998, Harris 1999). The surface brightness fluctuation method (Tonry & Schechter 1990, Hui *et al.* 1993) gives $(m - M)_0 = 27.78 \pm 0.10$, adjusted to the same M31 distance as above.

The number of stars *brighter* in I than the TRGB is very small: there are $\simeq 50$ objects in the CMD with $22.0 < I < 24.0$, i.e. about 0.5% of the total population. There will be four kinds of objects contributing to the numbers above the tip:

- (a) Accidental blends of bright RGB stars (Renzini 1998): using Renzini’s prescriptions, we can quickly show that the expected number of these blends is entirely negligible (there are ~ 1000 stars within about 1 mag of the RGB tip, spread over 1.9×10^6 pixels, giving $N_{blend} < 1$).
- (b) Giants or AGB stars in highly evolved states including the long-period-variable (LPV) or Mira states: the expected number of these is proportional to the total luminosity of the sampled stellar population. The integrated magnitude of all the stars in our sample brighter than $V = 27.5$ (roughly, the average completeness limit of the V photometry) is $V_{int} \simeq 17.72$. Using a normal Population II (globular cluster) luminosity function to extrapolate the luminosity function to fainter magnitude, we estimate very roughly that the total luminosity over all magnitudes is then $V_{int} \simeq 16.1$, equivalent to $L_{int} \simeq 5.9 \times 10^6 L_{\odot}$. Again using Renzini’s (1998) scaling relations, we would then expect to find ~ 10 LPV-type stars generated from the old-halo population within our field.
- (c) Foreground field stars, and any “starlike” background objects such as QSOs: over our small sampled area of 5.33 arcmin^2 , the number of objects in the latter category will be negligible. However, the predicted number of foreground stars in the range $I = 22 - 24$ (e.g., Bahcall & Soneira 1981) is $\simeq 5$ per arcmin^2 , which yields about 25 expected bright foreground stars across our field. This makes up about half the number of bright stars we see.
- (d) Any genuinely younger population of AGB stars: by process of elimination, we need to ascribe at most about 15 objects to this category; the other ~ 35 stars brighter than the RGB tip are accounted for as either LPVs or foreground stars.

We conclude that this part of the NGC 5128 halo is almost purely an “old” sample of stars; whatever recent star formation has affected the inner few kpc of the galaxy has not penetrated outward to contaminate this part of the halo.

5. Comparison With Other Galaxies

Most of the direct color-magnitude data currently available on halo populations in other galaxies is for Local Group systems such as M31 (Mould & Kristian 1986, Pritchett & van den Bergh 1988, Davidge 1993, Armandroff et al. 1993, Durrell et al. 1994, Reitzel et al. 1998), M33 (Mighell & Rich 1995, Mould & Kristian 1986), and the dwarf ellipticals including NGC 147 (Han et al. 1997), M32 (Grillmair et al. 1996), and NGC 185 (Martinez-Delgado & Aparicio 1998). With the HST cameras, such efforts have extended beyond the Local Group to include the previously discussed short-exposure study of NGC 5128 (Soria et al.

1996), two dwarf spheroidal companions of M81 (Caldwell et al. 1998), and the S0 galaxy NGC 3115 (Elson 1997). But, with the possible exception of NGC 3115, no other galaxy halo shows the same range of heavy element enrichment that we see in NGC 5128 amongst its old stars.

In Figure 8 we have plotted $I, (V - I)$ CMDs for our data along with three of the small ellipticals, NGC 147 and the two M81 dwarfs. Marked on each graph are the number of objects plotted and the fiducial lines for the most metal-poor and metal-rich globular clusters (M15 and NGC 6553). We note first, of course, that the NGC 5128 data exhibit by far the greatest color span of any of the four. Second, in relative numbers, NGC 5128 has the fewest stars *above* the TRGB. NGC 147 and M81-BK5N are quite similar to NGC 5128 in the location of the blue edge of the CMD, suggesting their original halo gas started with nearly primordial compositions; NGC 5128, however, has gone very much farther up the enrichment ladder. The CMD for the halo of NGC 5128 *is the first clear demonstration that giant E galaxies can possess extremely low-metallicity stars* as well as high-metallicity ones.

The only other galaxy mentioned above which may show a comparably broad abundance distribution is the S0 galaxy, NGC 3115 (Elson 1997). But NGC 3115 is more than 2 magnitudes more distant, with $I_{TRGB} \sim 26.0$. Consequently, the CMD in Elson’s study covers only the top part of the RGB, where the evolutionary tracks spread out rapidly with metallicity and where it is hardest to deduce the actual metallicity range and MDF. An additional factor hampering the interpretation of the NGC 3115 data is that its exposure time in V was only $\sim 2/3$ of that in I and, consequently, the very reddest stars ($V - I > 3$) have much more uncertain colors or are cut off entirely by the photometric incompleteness limit (see Figure 3 once again). The same was true to a somewhat lesser degree for the Soria et al. study of an inner-halo field in NGC 5128. Since their results cover only the top ~ 1.5 mag of the giant branch, their CMD clearly shows the metal-poor population, but (as they discuss), they can only place lower limits on the numbers of reddest stars. Even in our data, which cover ~ 3 magnitudes of the RGB, the very reddest stars fall below the $f = 0.9$ completeness line (Figure 3). These extremely red stars can be fully surveyed only by increased exposure time in the bluer filter.

It is intriguing to consider the possibility that an S0 galaxy (NGC 3115) might have experienced a heavy element enrichment and star formation history similar to that of a gE such as NGC 5128. Unfortunately, given the distance of NGC 3115 and current observational limitations, it is unlikely that we will be able to obtain data of the necessary quality for a rigorous comparison – or the giant ellipticals in Leo, Virgo, and Fornax – in the near future.

6. The Metallicity Distribution Function

A closer look at the color distribution is shown in Figure 9, where we have plotted histograms in $V - I$ for five magnitude intervals from $I = 24.0$ to 26.5 . The distribution is broadest at the top end where the evolutionary tracks are most separated, but it narrows in the lower bins to the point where the two faintest samples are strongly peaked. For NGC 3115, Elson (1997) suggests that the color distribution of the brightest halo stars is bimodal. In NGC 5128, we see no clear evidence for bi- or multi-modality in any of the color distributions; this does not, however, mean that the *metallicity* distributions are necessarily unimodal.

To derive the full MDF, we need to convert $(V - I)$ to $[\text{Fe}/\text{H}]$ on a star-by-star basis. The shape of the color histograms (Figure 9) does not give a correct indication of the MDF, since the conversion from color to metallicity is highly nonlinear, as is obvious in Figure 4. Ideally, to estimate metallicities we would prefer to use the fiducial tracks for the Milky Way globular clusters, which are on a well established and observationally based metallicity scale. However, most of the stars in NGC 5128 are clearly more metal-rich than our calibrators (47 Tuc, and even NGC 6553). Similarly, the observationally based conversion relations of Da Costa & Armandroff (1990) are valid only for $[\text{Fe}/\text{H}] \lesssim -0.7$ and thus irrelevant for NGC 5128.

To cover the full color range necessary, we have used a combination of the real cluster fiducial lines (all the ones shown in Figure 4) and the two most metal-rich isochrone lines shown in Figure 5. Although we regard this only as a preliminary procedure, the fact that the lower-metallicity isochrones agree closely in color with the globular cluster lines (noted above) gives some confidence that systematic errors in $[\text{Fe}/\text{H}]$ will not be serious.

In the brightest ~ 1 mag of the RGB, the tracks have strong curvature and interpolation between them is extremely sensitive to small errors in color. We have therefore chosen simply to avoid this region of the CMD, which in any event contains only a minority of the stars. Instead, we use only the data points further down the giant branch in the range $25.0 \lesssim I \lesssim 26.5$ where the tracks are more nearly vertical and interpolation between them is more reliable. For each star in this range, we then (a) determined the $(V - I)$ color of each fiducial line at the I magnitude of the star, and (b) interpolated in the $((V - I), [\text{Fe}/\text{H}])$ relation at that magnitude to predict $[\text{Fe}/\text{H}]$ for the given star.¹ A very similar procedure

¹Over the full range of metallicities shown here, the conversion is highly nonlinear. Simple linear interpolation between $(V - I)$ and $[\text{Fe}/\text{H}]$ within any pair of the fiducial lines produces systematic errors which show up as artificial “blocks” of stars in the $[\text{Fe}/\text{H}]$ histogram. To circumvent this, for each star we first calculated a hyperbola-like function of color, $C = ((V - I) - (V - I)_{min} + 1)^{-2.6}$ where $(V - I)_{min}$

was used by Grillmair et al. (1996) in their study of M32 to develop a rough histogram of metallicity from the CMD.

The resulting metallicity distribution is displayed in Figure 10, for three 0.5-magnitude ranges along the RGB. All three plots show a broad, shallowly sloped distribution at low metallicity, then a sharp rise near $[\text{Fe}/\text{H}] = -0.6$ to a peak near $\simeq -0.3$. Very few stars lie above solar metallicity. The overall shape of this distribution cannot be easily described as “bimodal” in the conventional sense, though it clearly has at least two major components. The approximate internal uncertainties in $[\text{Fe}/\text{H}]$ (shown in the top panel, for $I \simeq 25.5$) are, as expected, greatest at low metallicity where the isochrones are closest in color for a given $\Delta[\text{Fe}/\text{H}]$. Fortunately, this low-metallicity region of the MDF is least affected by the random photometric scatter because of its shallow slope; and in the more rapidly changing high-metallicity component, the photometric scatter has an intrinsically smaller effect. Before we continue, we need to consider two potential sources of systematic error in the overall shape of the distribution:

(a) Asymptotic-branch (AGB) stars must be present along with the first-ascent red giants that we are interested in. Since they are always bluer at a given metallicity, they will cause us to overestimate the relative numbers at the low-metallicity end. At the luminosity levels represented here (1 to 2 mag below the TRGB), the AGB tracks are $\simeq 0.05 - 0.10$ bluer in $(V - I)$ than the RGB (Bertelli et al. 1994). Inspection of the lifetimes along the evolutionary tracks shows that, over the range $25 < I < 26$, about $(20 \pm 3)\%$ of our total sample will be AGBs stars, nearly independent of metallicity. Their presence will therefore not dramatically skew the MDF (see below).

(b) As was noted earlier, a bias against the relative numbers of stars at the extreme red end is introduced by the photometric completeness line, which slants upward through the red tip of the RGB (Figure 3). We have already argued that this bias is considerably smaller in our data than in Soria et al. (1996) or in Elson (1997) because we reach much further down the giant branch. In addition, the fact that there is a clear gap in the CMD between the red edge of the RGB population and (e.g.) the 50% completeness limit in Figure 3 suggests that there are genuinely few stars more metal-rich than approximately solar abundance. However, close comparison with the isochrone lines suggests that we will be slightly underestimating the *relative* numbers of stars more metal-rich than $[\text{Fe}/\text{H}] \simeq -0.2$. Correcting for this would extend the upper envelope of the MDF in Figure 10 but would

is the color of the bluest fiducial line at the given I magnitude. Numerical trials showed that this C index was nearly a linear function of $[\text{Fe}/\text{H}]$ over our magnitude range of interest, allowing interpolation which was much more accurate and which did not generate artifacts in the MDF. This index was used purely for numerical convenience and is not suggested to have any physical significance.

not change the peak location.

For the present, we have not attempted to correct for either of these minor effects quantitatively, and we repeat that we consider the MDF derived here to be only a preliminary one. Ultimately, a better procedure for extracting the $[\text{Fe}/\text{H}]$ distribution would be to use a finer grid of fiducial RGB and AGB lines and an assumed input MDF to synthesize the observed color-magnitude array, appropriately convolved with the photometric error and completeness functions (cf. Martinez-Delgado & Aparicio 1998 for an example of this technique). We are currently exploring this approach.

The general shape of the MDF in Figure 10 is quite similar in all three magnitude bins, indicating that the $(V - I)$ to $[\text{Fe}/\text{H}]$ conversion was internally consistent. The faintest of the three magnitude bins ($I = 26.0 - 26.5$) is, however, clearly broader than the two brighter ones, a direct result of the increased random photometric errors there. For the purposes of the present discussion, we exclude this faintest bin, combining only the two brighter ones in which the internal photometric scatter does not exert an important effect on the internal spread of the MDF. The resulting composite MDF of 4514 stars is shown in Figure 11 (upper panel). The “metal-rich” component ($[\text{Fe}/\text{H}] \gtrsim -0.7$) contains $\simeq 64\%$ of the stars in the distribution. This dominant section of the MDF is reasonably matched by a simple Gaussian curve (shown in Figure 11) with a narrow dispersion $\sigma[\text{Fe}/\text{H}] \simeq 0.22$ and a maximum at $[\text{Fe}/\text{H}]_{peak} \simeq -0.32$.

At lower metallicities, we see the very extended and less populous component (36% of the total) sloping away to $[\text{Fe}/\text{H}] \sim -2$ and below. The upper part of this section (from $[\text{Fe}/\text{H}] \sim -1.1$ to -0.7) will be slightly contaminated by AGB stars from the metal-rich component itself; taking into account the behavior of the translation from $(V - I)$ to $[\text{Fe}/\text{H}]$, we estimate very roughly that 50 to 100 of the ~ 600 stars in this intermediate $[\text{Fe}/\text{H}]$ range will be AGB stars that have bin-jumped from the higher-metallicity component. Thus in relative terms, the histogram near $[\text{Fe}/\text{H}] \sim -1$ is about 10% higher than it should be. This offset will not affect any of the following discussion critically.

The mean abundance of the entire sample of stars, combining both components, is $\langle Z \rangle = (0.39 \pm 0.02)Z_{\odot}$ or $\langle [\text{Fe}/\text{H}] \rangle = -0.41 \pm 0.03$. Adjustment for the second-order bias corrections mentioned above would raise this mean even higher, perhaps by ~ 0.1 dex. This metallicity level is high for such a remote halo location, but is not inconsistent with the integrated colors and spectral parameters for E galaxies in general, which usually yield rather modest radial metallicity gradients and mean values in the range of $[\text{Fe}/\text{H}] \sim -0.4$ to above-solar (e.g. Thomsen & Baum 1989, Kormendy & Djorgovski 1989). Thus, our data strongly support the view that the problem of producing high-metallicity stars at extreme outer-halo distances is a generic one for ellipticals.

The only surface photometry for NGC 5128 extending to large radii ($r \simeq 10'$) is from van den Bergh (1976), based on UBV photoelectric photometry. Although his outermost points are at only half the projected radius of our field, they provide a useful comparison. Using the conversion relation of Couture et al. (1990) to translate integrated color roughly to metallicity, $(B - V)_0 = 0.200[\text{Fe}/\text{H}] + 0.971$, we find $[\text{Fe}/\text{H}] \sim 0.0 \pm 0.5$ for fields $8' - 10'$ from the center, in satisfactory agreement with the much more accurate mean metallicity we have calculated directly from the MDF.

Lastly, in Figure 12, we have replotted the MDF on a linear scale (number per unit abundance Z/Z_\odot , where we adopt $Z_\odot = 0.017$ as the solar abundance). In this graph, the dominance of the metal-richer population, and the small true range in abundance of the metal-poor component, are more clearly visible.

7. Discussion: Implications for Galaxy Evolution

The full MDF undoubtedly conceals many details of the enrichment history for NGC 5128 and, at this stage, we can provide only a rough interpretation. However, the overall shape of the MDF already indicates that a monolithic, single-burst formation event is unlikely to be an appropriate scenario for this galaxy.

7.1. Self-Contained Formation Scenarios

We first attempt to interpret the MDF in the context of an *in situ* formation picture: that is, we suppose that the galaxy was built primarily out of gas within its original protogalactic potential well, without important later additions from outside. Of course, this assumption cannot be strictly correct, since an accretion event with infalling gas and recent star formation is going on now, and other such events may have happened previously. Nevertheless, the general shape of the MDF can be matched surprisingly well by a combination of just two major star-forming phases: an initial one producing about one-third of the stars, starting from primordial (essentially unenriched) gas; and a later, more prominent phase producing two-thirds of the halo and with its maximum contribution at $Z \sim 0.5Z_\odot$.

A quantitative match to the MDF is shown in Figure 13, based on the classic picture of closed-box, one-zone chemical enrichment (e.g., Pagel & Patchett 1975). In these models the cumulative distribution of stellar abundance Z is given by

$$N(Z) \sim \text{const} (1 - e^{-(Z-Z_0)/y})$$

where N is the number of stars with heavy-element abundance less than Z ; the initial (pre-enriched) abundance of the gas is Z_0 ; and the yield rate is y . In Figure 13, the model curve for the lower-metallicity component has $(Z_0, y) = (0, 0.002)$, while the same quantities for the higher-metallicity component are $(0.003, 0.005)$. Although these particular parameters are only illustrative – other combinations with roughly similar values can be found which give similarly accurate fits – the overall quality of the match to the data is remarkable even with these very basic assumptions.

Within the context of this model, we would conclude that the first round of star formation proceeded at rather low global efficiency and low yield, leaving most of the gas unused till later. Exactly when and how these two epochs took place is still a matter of speculation (the MDF itself gives little direct information on timescales), but contemporary galaxy formation modelling may provide some guidance. In standard cold dark matter cosmologies, large galaxies are generally thought to have formed from hierarchical merging of dwarf-sized clumps which appear naturally within N-body simulations of galaxy formation (e.g., Frenk et al. 1988, Navarro & Benz 1991, Lacey & Cole 1994, Quinn et al. 1996, Navarro & Steinmetz 1997, Weil et al. 1998, among many others) and which are also postulated on observational grounds to be the sites of early globular cluster formation (Searle & Zinn 1978, Harris & Pudritz 1994). We can then imagine that the first burst of star formation took place within these clumps, starting at very low metallicity and enriching the residual gas in the still-lumpy potential well of the proto-elliptical up to an intermediate level near $[\text{Fe}/\text{H}] \sim -0.7$. The first wave of supernovae and massive stars would have ejected much of the gas from the small local potential wells of these dwarf-sized fragments before it had a chance to form many stars. Later, as the partially enriched gas recollected in the now-complete galactic potential well, a second and more major star-forming epoch took place which generated the main stellar bulk of NGC 5128 and enriched it to near-solar abundance.

These two early phases laid down the dominant features of the halo that we now see. Later on, the galaxy may have built further by accretion (with one such event going on now), but these more recent events have plainly been most important in the inner few kpc, with the outer halo largely unaffected by them.

Interestingly, Grillmair et al. (1996) have found roughly similar features in the halo population of the small Local Group elliptical M32. Its MDF shows a metal-rich peak at $[\text{Fe}/\text{H}] \simeq -0.2$ very much like NGC 5128, but with an overall distribution that is somewhat narrower. The “tail” extending to lower $[\text{Fe}/\text{H}]$ is present in M32, but is less populous and does not seem to extend below about $[\text{Fe}/\text{H}] \sim -1.5$. Just as we find here, Grillmair *et al.* note that a single one-zone model does not fit the total MDF; a combination of at least

two separate enrichment events is necessary, or some more complex history. Although NGC 5128 and M32 by no means represent the full range of ellipticals, it may not be premature to treat them as the first examples of a general pattern for such galaxies.

7.2. Connections with the Globular Cluster System

An additional important piece of evidence is shown in Figure 11b. Here, we show the MDF for the *globular clusters* in the halo of NGC 5128 (Harris et al. 1992; the cluster metallicity measurements are based on the sensitive Washington indices, principally $(C - T_1)$). This sample comprises 47 clusters with projected distances $4' < r < 22'$ from the center of NGC 5128; although they are located all over the halo, the globular cluster system has no significant metallicity gradient outside the central region (Harris et al. 1992), so the MDF shown here is quite representative of the clusters anywhere in the halo. Figure 11b displays the well known bimodal shape of the MDF seen in the globular clusters of several giant ellipticals as well as large disk galaxies. For our purposes, a remarkable feature of this plot is that the MDF of the *metal-rich* clusters *exactly coincides in peak location and dispersion* with the metal-rich stars, to well within the observational uncertainties. We suggest from this evidence that the metal-richer stars and globular clusters formed together, and that both represent the same generic population that makes up the main bulk of the galaxy.

Still another remarkable point of comparison is that for the clusters, the metal-richer component makes up only $\simeq 40\%$ of the total cluster population, while the metal-poor component is 60% of the total. These proportions are almost the reverse of the numbers for the halo *stars*. *If* we can safely associate the metal-poor clusters with the metal-poor stellar component (even though their MDFs have rather different shapes), these ratios imply that the *globular cluster specific frequency* S_N (the number of globular clusters per unit galaxy luminosity; Harris 1991) is $\simeq 2.8$ *times higher in the metal-poor component than in the metal-rich component*. Using the fact that the global specific frequency for the galaxy is $S_N(\text{tot}) = 2.6 \pm 0.6$ (Harris et al. 1998c), we can then derive specific frequencies separately for the metal-poor and metal-rich populations. These are $S_N(\text{MPP}) \simeq 4.3$ and $S_N(\text{MRP}) \simeq 1.5$. The former value is similar to the more cluster-rich ellipticals in Virgo and Fornax, while the latter is closer to the values for disk galaxies (Harris 1991).

A similar calculation has been done for the Virgo gE NGC 4472, where S_N for the metal-poor population is estimated to be more than an order of magnitude higher than for the metal-rich population (Lee et al. 1998, Forbes et al. 1997, Harris 1999). Within the context of *in situ* formation, we can speculate that the clusters formed very early on in

the first round of star formation, but that most of the gas which could have formed stars throughout the halo remained unused till the second round, leaving a low yield and high S_N as its distinctive traces. Harris *et al.* (1998c) have suggested that one mechanism which may have prevented the low-metallicity round of star formation from running to completion was the first burst of supernovae, igniting early enough that the proto-halo still had low overall density. We might also speculate that a high fraction of the gas had not yet collected into the dwarf-sized fragments within which star and cluster formation is believed to take place most efficiently.

We note that the formation picture we have just described – a two-phase *in situ* model with later minor effects from accretion and merger – is quite similar to the one developed by Forbes *et al.* (1997) from a comparison of the globular cluster systems in E galaxies. The MDF for the halo *stars* in this particular E galaxy provides a powerful new consistency test for this scenario.

7.3. Constraints on Accretions and Mergers

Can these new observations for NGC 5128 fit equally well into other formation scenarios? An interesting alternate picture for E galaxies is that of Côté *et al.* (1998), who suggest that the high-metallicity component was the main part of the original galaxy, while the low-metallicity component was acquired later on by a series of accretions of smaller satellites. Since smaller galaxies are more metal-poor, the relative number of low-metallicity stars would therefore increase with time, as long as the main process of accretion is “passive” (i.e., with low gas content and no new formation of stars). For NGC 5128, the accreted material would need to make up as much as one-third of the total galaxy, equivalent to about 200 dE galaxies averaging $M_V \simeq -15$ each. NGC 5128 is by far the largest galaxy in the sparse Centaurus group, so these numbers would require that it has already swallowed the great majority of the dwarf population that originally existed in the group. Currently the Centaurus group has about 20 dwarfs, mostly irregulars (Côté *et al.* 1997). Although accretion is obviously playing an ongoing role in the history of NGC 5128 at some level, these total numbers seem uncomfortably large if the entire metal-poor component of the MDF is to be explained this way. In addition, the specific frequency for the metal-poor component is like that of normal cluster-rich dwarf ellipticals (Durrell *et al.* 1996) rather than cluster-poor dwarf irregulars, so we would have to postulate that the metal-poor component of NGC 5128 was built up mostly by accreting dE’s. But dwarf irregulars vastly outnumber dE’s in most small galaxy groups like Centaurus. Thus *a priori* it is much more probable that NGC 5128 would have built up a metal-poor halo with *low*

specific frequency, contrary to what we see.

Finally, it is not clear that a combination of many dwarfs of various sizes and individual enrichment histories would produce an MDF with the simple shape that we see (basically well matched by a single enrichment event starting from primordial composition). It is perhaps noteworthy that the MDF for the Milky Way halo has a roughly symmetric shape centered on $[\text{Fe}/\text{H}] \sim -1.7$ (e.g., Laird et al. 1988), rather unlike the metal-poor component in NGC 5128.

A possible counterargument to the rather simple calculation just outlined above is that it may seriously overestimate the fraction of the *whole* galaxy made up by the metal-poor component. Our one target field is located well out in the halo, where presumably the relative numbers of metal-poor stars are largest. If we were able to sample the MDF over all radii, the ratio of metal-rich to metal-poor components $N(\text{MRC})/N(\text{MPC})$ might reasonably be expected to increase inward; or, at smaller radii ($r \lesssim 5$ kpc, the region most affected by later accretions of gas-rich satellites), we might expect to see the emergence of a third and still more metal-rich component that was built up through later star formation in the central bulge. However, in this case the specific frequency problem with the globular cluster system would become even worse. If, for example, the global value of $N(\text{MRC})/N(\text{MPC})$ is ~ 0.1 instead of ~ 0.3 , then we would have $S_N(\text{MPC}) \simeq 12$, bringing it up into the realm of the high- S_N galaxies like M87 and the central cD’s in rich clusters (Harris et al. 1998c). Passive accretion of dwarf galaxies, each of which has $S_N \sim 1 - 6$, seems highly unlikely to yield such a result.

More or less the opposite approach is taken in the merger model of Ashman & Zepf (1992). Here, the metal-rich component is assumed to form during the merger of very gas-rich progenitor galaxies. The merger-driven star and cluster formation is postulated to occur predominantly in the central regions where the gas collects most strongly, while the metal-poor component represents the combined halos of the original pre-merger objects. However, part of the Ashman & Zepf (1992) picture is that the metal-rich component should have *high* specific frequency (i.e. that globular clusters are postulated to form more efficiently in the colliding gas clouds). This is, unfortunately, exactly the opposite of what we find in NGC 5128, where $S_N(\text{MRC})$ is several times smaller than in a typical gE. In addition, we clearly find that the metal-rich component represents *most* of the galaxy even far out in the halo, and not just a minor addition. In this view, we would have to assume that the pre-merger “galaxies” were themselves almost entirely gaseous, which in our view considerably blurs the distinction between a merger and *in situ* formation picture to begin with.

No single model is fully satisfactory or fully quantitative at present. Nevertheless,

we believe that a plausible explanation of the data for NGC 5128 is that the bulk of the galaxy was built during two rather distinct star-forming epochs, from an original supply of gas within its global potential well. Later accretions of satellites have probably made minor additions to the total mass, particularly in the central regions. We also suggest that a better assessment of the various models will be possible once we can sample the stellar MDF at several different places in the halo and measure its radial gradient.

8. Summary

We have used WFPC2 photometry to derive a color-magnitude diagram for the halo stars in NGC 5128, reaching almost 3 magnitudes down the giant branch. We find that the stellar population is completely dominated by a classic old RGB population, with negligible contribution from any younger bright AGB component. The metallicity range of the stars is extremely broad, extending from $[\text{Fe}/\text{H}] \lesssim -2$ to above-solar abundance. The mean metallicity of the entire sample is $\langle [\text{Fe}/\text{H}] \rangle = -0.41$.

From the CMD and the fiducial isochrone lines, we have generated a first-order measurement of the metallicity distribution function for the RGB stars, the first such data for any giant elliptical galaxy. The MDF is well matched by a remarkably simple model with two distinct phases of chemical enrichment. In addition, we find that the metal-richer component (which makes up two-thirds of all the stars) has the same peak location and metallicity dispersion as the metal-richer *globular clusters* in the halo of NGC 5128, suggesting strongly that both types of objects formed together. The match between the more metal-poor stars and metal-poor globular clusters is less exact. However, the *specific frequencies* of the two components are strikingly different: the metal-poor component produced almost three times more globular clusters per unit halo light than the metal-rich component.

Comparing different formation scenarios for E galaxies (*in situ*, accretion, mergers) with the combined observations from the halo stars and the globular clusters, we suggest that the most satisfactory description is a two-phase *in situ* model, in which an early, widely dispersed burst of star formation starting from primordial material left behind the metal-poor stellar component, but also left most of the original gas supply unused. Then, a second and more major burst took place, giving rise to the metal-rich component which forms the majority of the stars. Models in which (for example) the metal-poor component was accreted later, or in which the metal-rich component was formed in mergers, are clearly less satisfactory.

NGC 5128 is becoming a rich mine for stellar population studies that will help us reconstruct its formation history. Further observational steps can easily be made which will add new dimensions to its study: for example, additional HST photometry to the same depth that we have used here, at different radial locations in the halo, would allow us to measure the radial metallicity gradient and the progressive change in the entire MDF. Eventually, with more advanced imaging tools, we can look forward to obtaining far larger samples of stars, penetrating further down the color-magnitude diagram to the horizontal branch and below, and finding fine structure in the metallicity distribution function which will lead to more advanced modelling.

This work was supported financially through the Natural Sciences and Engineering Research Council of Canada, through research grants to G.L.H.H. and W.E.H.

REFERENCES

- Armandroff, T. E., Da Costa, G. S., Caldwell, N., & Seitzer, P. 1993, *AJ*, 106, 986
- Ashman, K. M. & Zepf, S. E. 1992, *ApJ*, 384, 50
- Bahcall, J. N., & Soneira, R. M. 1981, *ApJS*, 47, 357
- Bertelli, G., Bressan, A., Chiosi, C., Fagotto, F., & Nasi, E. 1994, *A&AS*, 106, 275
- Brodie, J. P., & Huchra, J. P. 1991, *ApJ*, 379, 157
- Burstein, D. & Heiles, C. 1984, *ApJS*, 54, 33
- Caldwell, N., Armandroff, T. E., Da Costa, G. S., & Seitzer, P. 1998, *AJ*, 115, 535
- Christian, C. A. & Heasley, J. N. 1991, *AJ*, 101, 848
- Côté, P., Marzke, R. O., & West, M. J. 1998, *ApJ*, 501, 554
- Côté, S., Freeman, K. C., Carignan, C., & Quinn, P. J. 1997, *AJ*, 114, 1313
- Couture, J., Harris, W. E., & Allwright, J. W. B. 1990, *ApJS*, 73, 671
- Da Costa, G., & Armandroff, T. 1990, *AJ*, 100, 162
- Davidge, T. J. 1993, *ApJ*, 409, 190
- Durrell, P. R., Harris, W. E., and Pritchett, C. R. 1994, *AJ*, 2114
- Durrell, P. R., Harris, W. E., Geisler, D., & Pudritz, R. E. 1996, *AJ*, 112, 972
- Ebner, K., & Balick, B. 1983, *PASP*, 95, 675
- Elson, R. A. W. 1997, *MNRAS*, 286, 771
- Fernley, J. et al., 1998, *A&A*, 330, 515
- Forbes, D., Brodie, J. P., & Grillmair, C. J. 1997, *AJ*, 113, 1652
- Frenk, C. S., White, S. D. M., Davis, M., & Efstathiou, G. 1988, *ApJ*, 327, 507
- Graham, J. A. 1979, *ApJ*, 232, 60
- Gratton, R. G., Fusi Pecci, F., Carretta, E., Clemintini, G., Corsi, C. E., & Lattanzi, M. 1997, *ApJ*, 491, 749

- Grillmair, C. J., et al. 1996, AJ, 112, 1975
- Guarnieri, A., Clementini, G., Valentini, G., Castro-Tirado, A., Gorosabel, J., & Pedrosa, A. 1998, A&A, 331, 70
- Han, M. et al., 1997, AJ, 113, 1001
- Harris, G. L. H., Geisler, D., Harris, H. C., & Hesser, J. E. 1992, AJ, 104, 613 (HGHH)
- Harris, G. L. H., Poole, G. B., & Harris, W. E. 1998a, AJ, 116, in press
- Harris, H. C., Harris, G. L.H., Hesser, J. E., & MacGillivray, H. T. 1984, ApJ, 287, 185
- Harris, W. E. 1991, ARA&A, 29, 543
- Harris, W.E. 1999, in Star Clusters, Saas-Fee workshop, in press
- Harris, W. E., Durrell, P. R., Pierce, M. J., & Secker, J. 1998b, Nature, 395, 45
- Harris, W. E., Harris, G. L. H., & McLaughlin, D. E. 1998c, AJ, 115, 1801
- Harris, W. E., & Pudritz, R. E. 1994, ApJ, 429, 177
- Hesser, J. E., Harris, H. C., & Harris, G. L. H. 1986, ApJ, 303, L51
- Holtzman, J. A., Burrows, C. J., Casertano, S. Hester, J. J., Trauger, J. T., Watson, A. M., and Worthey, G. 1995, PASP, 107, 1065
- Hui, X., Ford, H. C., Ciardullo, R., & Jacoby, G. H. 1993, ApJ, 414, 463
- Hui, X., Ford, H. C., Freeman, K. C., & Dopita, M. A. 1995, ApJ, 449, 592
- Kormendy, J., & Djorgovski, S. 1989, ARA&A, 27, 235
- Lacey, C., & Cole, S. 1994, MNRAS, 271, 676
- Laird, J. B., Carney, B. W., Rupen, M. W., & Latham, D. W. 1988, AJ, 96, 1908
- Lee, M. G., Freedman, W. L., & Madore, B. F. 1993, ApJ, 417, 553
- Lee, M. G., Kim, E., & Geisler, D. 1998, AJ, 115, 947
- Madore, B. F. & and Freedman, W. L. 1995, AJ, 109, 1645
- Martinez-Delgado, D., & Aparicio, A. 1998, AJ, 115, 1462
- Mighell, K. J., Rich, R. M. 1995, AJ,110, 1649

- Mould, J. & Kristian, J. 1986, ApJ, 305, 591
- Navarro, J. F., & Benz, W. 1991, ApJ, 380, 320
- Navarro, J. F., & Steinmetz, M. 1997, ApJ, 478, 13
- Pagel, B. E. J., & Patchett, B. E. 1975, MNRAS, 172, 13
- Pritchett, C. & van den Bergh, S. 1988, ApJ, 331, 135
- Quinn, T., Katz, N., & Efstathiou, G. 1996, MNRAS, 278, L49
- Reitzel, D. B., Guhathakurta, P., & Gould, A. 1998, AJ, 116, 707
- Renzini, A. 1998, AJ, 2459
- Sakai, S., Madore, B. F., and Freedman, W. L. 1996, ApJ, 461, 713
- Searle, L., & Zinn, R. 1978, ApJ, 225, 357
- Soria, R., Mould, J. R., Watson, A. M., Gallagher, J. S. III, Ballester, G. E., Burrows, C. J., Casertano, S., Clarke, J. T., Crisp, D., Griffiths, R. E., Hester, J. J., Hoessel, J. G., Holtzman, J. A., Scowen, P. A., Stapelfeldt, K. R., Trauger, J. T., & Westphal, J. A. 1996, ApJ, 465, 79
- Stetson, P.B. 1992, in *Astronomical Data Analysis Software and Systems I*, ASP Conf.Ser. Vol.8, edited by G.H.Jacoby (ASP, San Francisco), p. 289
- Storchi-Bergmann, T., Bica, E., & Kinney, A. L. 1997, MNRAS, 290, 231
- Thomsen, B., & Baum, W. A. 1989, ApJ, 347, 214
- Tonry, J. 1991, ApJ, 373, L1
- Tonry, J. L., & Schechter, P. L. 1990, AJ, 100, 1794
- van den Bergh, S. 1976, ApJ, 208, 673
- van den Bergh, S. 1995, ApJ, 446, 39
- Weil, M. L., Eke, V. R., & Efstathiou, G. 1998, MNRAS, in press
- Whitmore, B., & Heyer, I. 1997, Space Telescope Science Institute, Instrument Science Report 97-08

Fig. 1.— The south halo region of NGC 5128, showing the location of our WFPC2 field (labelled HHP) and the field studied by Soria et al. (1996, labelled S96). North is at top and East at left. Our field is located at a projected distance $R_{gc} = 18'32$ from the center of NGC 5128, equivalent to 20.8 kpc for a galaxy distance $d = 3.9$ Mpc.

Fig. 2.— A mosaic of our HST WFPC2 field. Note the globular cluster C44 (Harris et al. 1998a) at the center of the PC1 chip. The dark swaths across the lower right of PC1 are scattered light from a bright star off the edge of the field. This image is the combined sum of all 10 long exposures in V , totalling 12800 sec. The data presented here are the results from the WF2,3,4 fields. The directions (N,E) are only approximate; see the previous Figure.

Fig. 3.— *Upper panel:* The I vs. $V - I$ color-magnitude diagram for 10352 measured stars with good PSF fits ($\chi < 2$). The superimposed lines represent 90% (dashed) and 50% (solid) photometric completeness levels, as determined from artificial-star tests (see text). *Lower panel:* Error bars showing the photometric measurement uncertainty as a function of magnitude and color.

Fig. 4.— The color-magnitude diagram from Figure 3, with fiducial lines of four Galactic globular clusters superimposed. These are M15 ($[Fe/H] = -2.2$), NGC 1851 ($[Fe/H] = -1.3$), 47 Tuc ($[Fe/H] = -0.7$) from Da Costa & Armandroff (1990), and NGC 6553 ($[Fe/H] = -0.25$) from Guarnieri et al. (1998). The NGC 5128 halo stars cover an extremely wide metallicity range.

Fig. 5.— The color-magnitude diagram from Figure 3, with theoretical isochrone lines from Bertelli et al. 1994 superimposed. The isochrones have an age of 12.5 Gyr and metallicities as labelled from -1.6 to $+0.5$.

Fig. 6.— The same as Figure 5, except that the theoretical isochrones are for the same metallicity ($[Fe/H] = -0.32$) and a range of ages from 5 to 18 Gyr.

Fig. 7.— The luminosity function for the NGC 5128 red giant branch. The hatched region is for the 4120 stars more metal-poor than $[Fe/H] = -0.7$, while the clear region is for all data (10352 stars). The adopted level of the RGB tip at $I = 24.1 \pm 0.1$ is indicated.

Fig. 8.— $I, (V - I)$ CMDs for NGC 5128 (this paper), the Local Group dwarf elliptical NGC 147 (Han et al. 1997), and two dwarf ellipticals in the M81 group (Caldwell et al. 1998). The number of star in each CMD is labelled in the lower right corner of eac panel. Fiducial lines for the metal-poor globular cluster M15 and the metal-rich cluster NGC 6553, as in Fig. 4, are superimposed on each one. NGC 147 and M81-F8D1 have a modest mixture of low-to-intermediate metallicity, while the very small dwarf M81-BK5N is entirely metal-poor.

Fig. 9.— The $(V - I)$ color distribution across the giant branch of NGC 5128, in 0.5-magnitude bins from $I = 24.0 - 26.5$.

Fig. 10.— The $[\text{Fe}/\text{H}]$ metallicity distribution in three magnitude bins across the giant branch, obtained by interpolation within the fiducial RGB sequences as described in the text. Error bars in the top panel represent the uncertainties in $[\text{Fe}/\text{H}]$ resulting from the photometric measurement uncertainty in the $(V - I)$ colors.

Fig. 11.— *Upper panel:* The $[\text{Fe}/\text{H}]$ distribution for the two brightest samples in Fig. 10. *Lower panel:* The $[\text{Fe}/\text{H}]$ distribution for 47 globular clusters in the halo of NGC 5128 (Harris et al. 1992). The Gaussian curves superimposed on the metal-rich components in each graph have identical means $[\text{Fe}/\text{H}](\text{peak}) = -0.32$ and dispersions $\sigma = 0.22$.

Fig. 12.— The metallicity distribution function from Fig. 11, replotted as the number of stars per unit linear abundance Z/Z_{\odot} .

Fig. 13.— Metallicity distribution function from Figure 11, fitted by a two-component enrichment model as described in the text. The low-metallicity component has an initial abundance $Z_0 = 0$ and a yield $y = 0.002 \simeq 0.12Z_{\odot}$. The high-metallicity component has an initial abundance $Z_0 = 0.003$ (equivalent to $[\text{Fe}/\text{H}] \simeq -0.75$) and a yield $y = 0.005$.

This figure "Harris.fig1.jpg" is available in "jpg" format from:

<http://arxiv.org/ps/astro-ph/9810134v1>

This figure "Harris.fig2.jpg" is available in "jpg" format from:

<http://arxiv.org/ps/astro-ph/9810134v1>

This figure "Harris.fig3.jpg" is available in "jpg" format from:

<http://arxiv.org/ps/astro-ph/9810134v1>

This figure "Harris.fig4.jpg" is available in "jpg" format from:

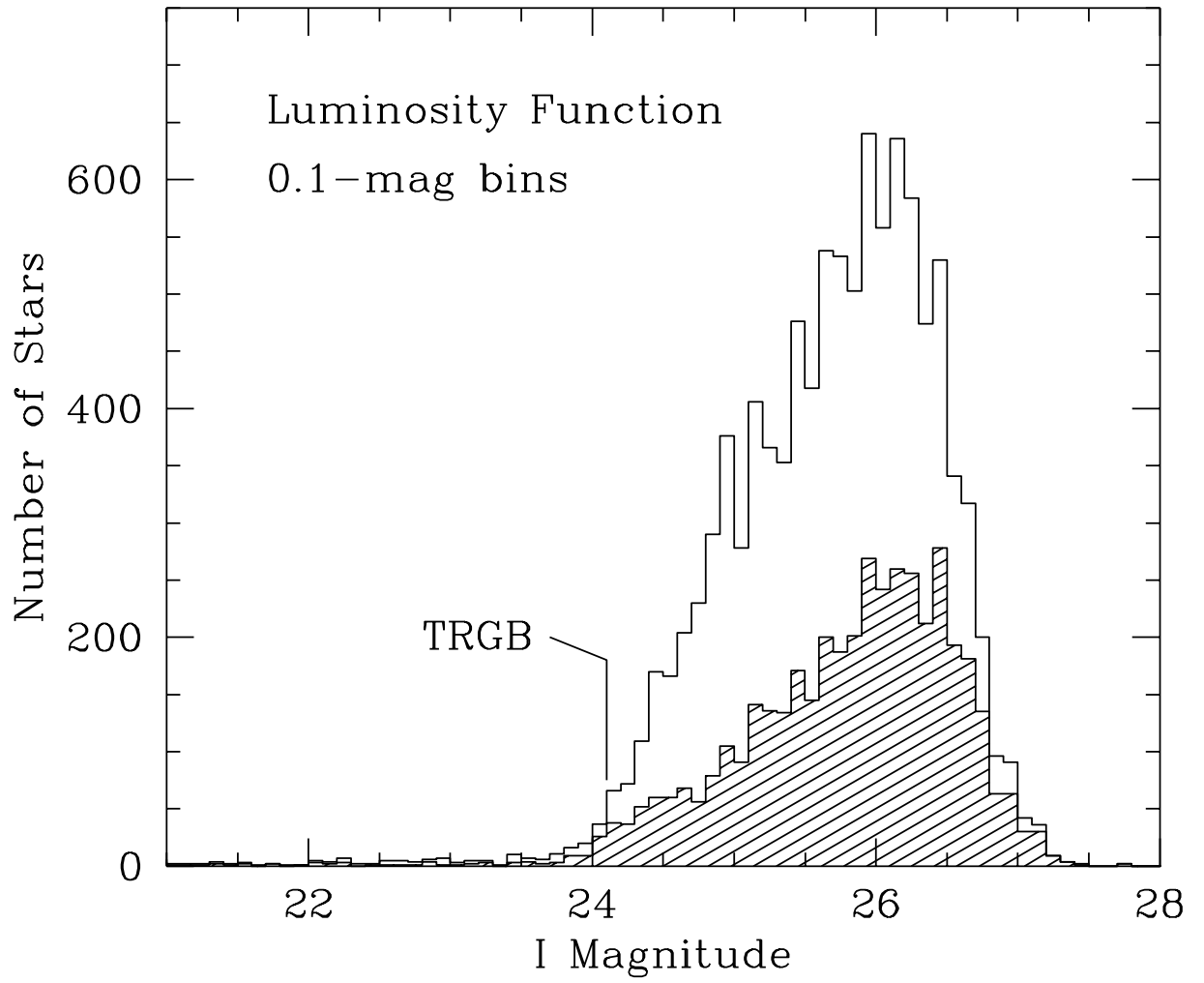
<http://arxiv.org/ps/astro-ph/9810134v1>

This figure "Harris.fig5.jpg" is available in "jpg" format from:

<http://arxiv.org/ps/astro-ph/9810134v1>

This figure "Harris.fig6.jpg" is available in "jpg" format from:

<http://arxiv.org/ps/astro-ph/9810134v1>



This figure "Harris.fig8.jpg" is available in "jpg" format from:

<http://arxiv.org/ps/astro-ph/9810134v1>

